Effects of polymer microstructure introduced by radical ring-opening polymerization on nanoencapsulation and controlled release

Polymer 307 (2024) 127284

Contents lists available at ScienceDirect

Polymer

journal homepage: www.elsevier.com/locate/polymer

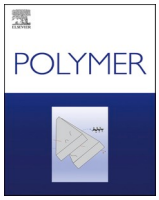

Effects of polymer microstructure introduced by radical ring-opening polymerization on nanoencapsulation and controlled release

Algin Oh Biying [a,1], Srinivasa Reddy Mothe [a,1], Alexander W. Jackson [a], Parijat Kanaujia [a], Praveen Thoniyot [a,b,*]

[a] Institute of Sustainability for Chemicals, Energy and Environment (ISCE2), Agency for Science, Technology and Research (A*STAR), 1 Pesek Road, Singapore, 627833, Republic of Singapore

[b] Department of Chemical Engineering and Chemistry, Institute for Complex Molecular Systems, Eindhoven University of Technology, P.O. Box 513, 5600 MB, Eindhoven, the Netherlands

ARTICLE INFO

Keywords:
Amphiphilic diblock copolymers
mPEG-*b*-PCL
mPEG-*b*-PMDO
rROP
RAFT-Mediated rROP
Encapsulation
Nanoparticles (NPs)
Crystallinity
Branching
Controlled release

ABSTRACT

In this study, the effect of the polymer structural difference introduced by radical ring-opening polymerization (rROP) of a cyclic ketene acetal (CKA) monomer, analogous to ε-caprolactone (CL), on the nanoencapsulation and controlled release of hydrophobic actives curcumin and fenofibrate was explored. The two chosen polymers are amphiphilic diblock copolymers namely methoxy poly(ethylene glycol)-*b*-poly(ε-caprolactone) (mPEG-*b*-PCL) and methoxy poly(ethylene glycol)-*b*-poly(2-methylene-1,3-dioxepane) (mPEG-*b*-PMDO). Both polymers serve as a good comparison as they have a similar average molecular weight (M_n) and the same hydrophilic PEG chains with the main difference in microstructure of hydrophobic PCL and PMDO chains. Nuclear magnetic resonance spectroscopy (NMR) (^{1}H and ^{13}C), gel permeation chromatography (GPC), thermogravimetric analysis (TGA), differential scanning calorimetry (DSC) and X-ray diffraction (X-RD) confirmed the structures of the polymers. mPEG-*b*-PMDO possesses less crystallinity or is more amorphous as compared to the linear mPEG-*b*-PCL due to branching or polymer disorder in the hydrophobic segment as a result of radical mechanism operating in rROP. The subsequent nanoencapsulation of hydrophobic active curcumin with mPEG-*b*-PMDO yielded higher loading content (LC) and encapsulation efficiency (EE) in the hydrophobic core of the nanoparticle (NP) due to more hydrophobic interactions between hydrophobic core and hydrophobic active. In contrast, lower LC and EE were observed for the nanoencapsulation of fenofibrate with mPEG-*b*-PMDO. The further release experiments were carried out in the aqueous and hydro-alcoholic systems over a period of 24 h at 37 °C. These experiments further supported our hypothesis regarding the influence of polymer structure, revealing slower, controlled, and more consistent release profiles for both curcumin and fenofibrate with mPEG-*b*-PMDO compared to mPEG-*b*-PCL. Our approach could open new opportunities for utilizing this polymer in personal care and biomedical applications.

1. Introduction

One of the well-known routes to improve the bioavailability of hydrophobic drugs is through encapsulation by using various drug carriers such as liposomes [1], polymeric micelles [2], drug-polymer conjugates [3], microparticles [4], nano-associates [5], nanoparticles (NPs) [6] which can attain improved solubilization and controlled release of hydrophobic drugs [7–12]. Among them, NPs have been the object of growing scientific attention as they emerged as potential carriers for poorly water-soluble drugs. The nanostructures are formed through the self-assembly of amphiphilic block copolymers, where the hydrophobic segment of the polymer constitutes the core-shell structure. This arrangement enables the accommodation of hydrophobic actives within the inner core via physical entrapment [13], while the hydrophilic coronas stabilize the structure [14]. Given that hydrophobic actives can only be captured within the hydrophobic or amorphous regions of the

* Corresponding author. Institute of Sustainability for Chemicals, Energy and Environment (ISCE2), Agency for Science, Technology and Research (A*STAR), 1 Pesek Road, Singapore, 627833, Republic of Singapore.
E-mail address: p.thoniyot@tue.nl (P. Thoniyot).

[1] co-first authors.

https://doi.org/10.1016/j.polymer.2024.127284
Received 28 December 2023; Received in revised form 4 June 2024; Accepted 10 June 2024
Available online 12 June 2024

polymer particle, polymers with higher amorphous characteristics are anticipated to exhibit greater loading of actives [15].

Numerous polymer combinations consisting of hydrophilic and hydrophobic segments have been used in designing polymer NPs for various drug delivery applications [16,17]. Among these combinations, poly(ethylene glycol) (PEG) and poly(ε-caprolactone) (PCL) are the most commonly employed hydrophilic and hydrophobic blocks respectively because of their non-toxicity, biocompatibility and biodegradability characteristics. Another polyester similar to PCL is poly (2-methylene-1,3-dioxepane) (PMDO), which is an isomer of PCL. PCL and PMDO are typically synthesized through condensation polymerization and radical ring-opening polymerization (rROP) of cyclic monomers, ε-caprolactone (CL), and (2-methylene-1,3-dioxepane) (MDO), respectively (Scheme 1). Compared to traditional condensation polymerization methods, rROP offers a streamlined and efficient route to producing well-defined block copolymers with tailored properties. It provides greater versatility in incorporating various functional groups or targeting moieties into the polymer chains with precise molecular weights and low polydispersity, especially when employing xanthate-mediated rROP via reversible addition–fragmentation chain transfer (RAFT) technique [18–23]. Thus, it can be applied to a wider range of available comonomers. Moreover, rROP is a reproducible process and is suitable for industrial-scale production, as it can be easily adapted to batch or continuous processes. Since the pioneering work of Bailey et al. [24], the development of the PMDO has consistently attracted interest due to its unique branching structure [25]. This hydrophobic block, characterized by branching leading to increased amorphous character, facilitates increased hydrophobic interactions between the hydrophobic core and hydrophobic drugs, thereby enhancing drug loading capacity. Conversely, the PCL block exhibits a less amorphous or semi-crystalline nature, which may potentially reduce drug loading efficiency due to its lower hydrophobic interactions [26]. However, in scenarios involving planar molecular structures capable of intercalating between semi-crystalline polymer packing, higher encapsulation efficiency and active loading could be achieved [27].

Curcumin is a natural polyphenol extracted from the root of turmeric (*Curcuma longa* L., Zingeberaceae) [28]. Its lipophilic nature rendered it to be insoluble in water but soluble in other organic solvents such as ethanol and dimethylsulfoxide [29]. It has various health benefits due to its anti-inflammatory [30], anti-oxidant [31], anti-mutagenic [32], anti-microbial32 [33] and other therapeutic properties [29,34]. However, despite the various health benefits, they cannot be fully utilized due to rapid elimination and metabolism as well as poor absorption in the human body leading to its poor bioavailability [35]. Fenofibrate belongs to the derivative of fibric acid used primarily for lipid regulating [36]. It functions by controlling the triglyceride and cholesterol levels in blood plasma of patients at risk of cardiovascular disease [37,38]. Similar to curcumin, it has poor aqueous solubility and bioavailability which leads to less than desired therapeutic effectiveness [39]. Hence, designing of suitable delivery system which improves solubilization and bioavailability of such hydrophobic actives is essential.

In this study, we investigated the effect of the crystallinity of polymer structures on nanoencapsulation of both curcumin and fenofibrate actives. Two amphiphilic diblock copolymers with similar average molecular weight (M_n), mPEG-*b*-PCL (methoxy poly(ethylene glycol)-*b*-poly(ε-caprolactone)) and mPEG-*b*-PMDO (methoxy poly(ethylene glycol)-*b*-poly(2-methylene-1,3-dioxepane)) were chosen to compare on the loading efficiency and release study of actives in the aqueous and hydro-alcoholic system each at 37 °C over a period of 24 h mPEG-*b*-PMDO and mPEG-*b*-PCL have different degree of crystallinity due to the branching in PMDO which increases the amorphous character giving rise to higher incorporation of the drug in the hydrophobic core. Our objective is to design a pathway for improving the solubilization, encapsulation efficiency and controlled release parameters of the drug in different polyester-based systems. We hypothesize that introducing branching or enhancing hydrophobic character of the block copolymer via rROP in polyesters will facilitate the more hydrophobic interactions between hydrophobic drug and hydrophobic particle core and subsequently enable higher encapsulation efficiency and controlled release. We believe that in the realm of NP scale polymeric drug delivery systems, certain physical properties, such as a very high surface-to-volume ratio, confer stability upon colloids of polymeric NPs in aqueous or hydro-alcoholic conditions, thereby facilitating the consistent progression of drug delivery from the core of the NPs [40]. It is noteworthy that the composition of the polymer, particularly the balance between hydrophobic and hydrophilic functionalities, as exemplified in mPEG-*b*-PCL and mPEG-*b*-PMDO polymer backbones, plays a crucial role. This composition affects the solubilization of polymeric NPs and

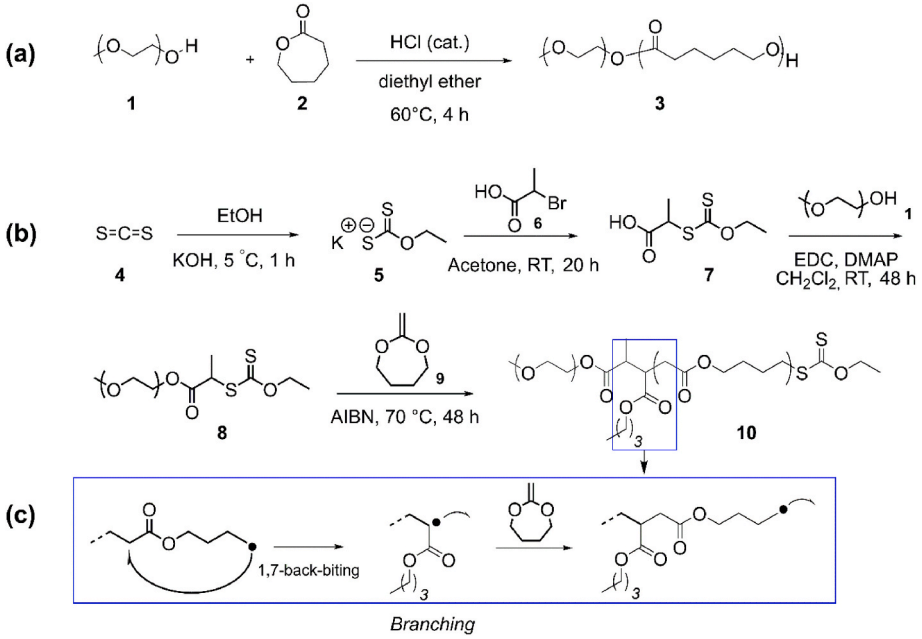

Scheme 1. Reaction schemes for the synthesis of mPEG-*b*-PCL and mPEG-*b*-PMDO (a) Acid-catalyzed ROP of ε-CL (b) RAFT-mediated rROP of MDO (c) Mechanism for the formation of branching in mPEG-*b*-PMDO.

subsequent drug release, often occur through diffusion mechanisms [41]. For instance, in both mPEG-*b*-PCL and mPEG-*b*-PMDO, hydrophilic and hydrophobic block ratios are nearly similar at 5000/7000 g/mol as determined by proton nuclear magnetic resonance spectroscopy (^{1}H NMR) (refer to Fig. 2b). However, despite the similarity in block ratios, it has been observed that mPEG-*b*-PCL renders the polymer more hydrophilic or crystalline, thereby enhancing its solubility in aqueous or hydro-alcoholic systems. This increased hydrophilicity promotes faster drug release through diffusion. Conversely, in mPEG-*b*-PMDO, characterized by a higher hydrophobic nature with branched structure, drug release occurs slowly and consistently through diffusion [42]. To our knowledge, this study represents the first direct comparison between PCL and its counterpart PMDO, both incorporated into amphiphilic diblock copolymers, regarding their ability to load and release drugs in a controlled manner from the particles they form when self-assembled. Our approach may create new possibilities for using these rROP-based copolymers instead of traditional polyesters in different drug delivery technologies within pharmaceutical and personal care chemical fields.

2. Results and discussion

It is widely accepted that the encapsulation of pharmaceutical molecules within polymeric delivery vehicles results in improved biodistribution and circulation times when compared to free drug molecules. Therefore, the ability to capture, stabilize and release plays an important role in designing such amphiphilic block copolymers. In this work, we designed and synthesized two diblock copolymers mPEG-*b*-PCL and mPEG-*b*-PMDO in which PEG, PCL, and PMDO have a comparable molecular weight (M_n) of 5000 and 7000 g/mol ($mPEG_{5k}$, PCL_{7k}, $PMDO_{6.3k}$) (Scheme 1). Both segments with similar molecular weights in each diblock copolymer provide a good comparison so that the effect of polymer structure could be analyzed easily.

2.1. Synthesis and characterization of diblock copolymers mPEG-b-PCL and mPEG-b-PMDO

mPEG-*b*-PCL (**3**) was synthesized via acid-catalyzed ROP of ε-CL (**2**) using hydrogen chloride (HCl) as the catalyst and $mPEG_{5k}$ (**1**) as the macroinitiator in diethyl ether at 60 °C for 4 h (Scheme 1a). Whereas mPEG-*b*-PMDO (**10**) was prepared from RAFT-mediated rROP of MDO (**9**) using AIBN (azobisisobutyronitrile) as the radical flux and $mPEG_{5k}$-xanthate (**8**) as the macroinitiator in bulk at 70 °C for 48 h (Scheme 1b). Macroinitiator $mPEG_{5k}$-xanthate was synthesized from the carbon disulfide (CS_2) and potassium hydroxide as initial starting materials in ethanol in a total of three steps. The progress of all reactions was determined by ^{1}H NMR analysis (Fig. 1). After completion of the reaction at their respective time, the final polymers were purified by precipitation from dichloromethane into hexane. As the precipitation is progressed, the high molecular weight polymer chains will crash out of the solution phase while keeping smaller molecular weight polymer chains in the solution as a dissolved state. This process was repeated 2–3 times by adding fresh hexane each time ensuring all reagents used in the polymerization were eliminated successfully prior to NMR analysis. Refer to pages S5–S7 in the supporting information (SI) for the detailed synthetic procedures for mPEG-*b*-PCL and mPEG-*b*-PMDO and their precursors.

The structural composition of blocks of mPEG-*b*-PCL and mPEG-*b*-PMDO were determined by NMR (^{1}H and ^{13}C) and the results are outlined in Fig. 1. From ^{1}H NMR of mPEG-*b*-PCL (**3**) in Fig. 1a, peaks *a*, *c*, *d* + *e* and *f* at 3.96, 2.20, 1.55 and 1.29 ppm respectively refer to methylene protons (–C(O)–CH$_2$–CH$_2$–CH$_2$–CH$_2$–CH$_2$–*O*-) of CL, whereas peak *b* at 3.55 ppm refers to methylene protons (-*O*-CH$_2$-CH$_2$-*O*-) of PEG. The peaks *d*-*f* are often observed as multiplets due to coupling with neighboring protons. The degree of polymerization (DP) in PEG and PCL blocks was determined by comparing the peak of the terminal methoxy group (CH$_3$–*O*–CH$_2$–CH$_2$–*O*-) of PEG, appearing at 3.27 ppm, with peak

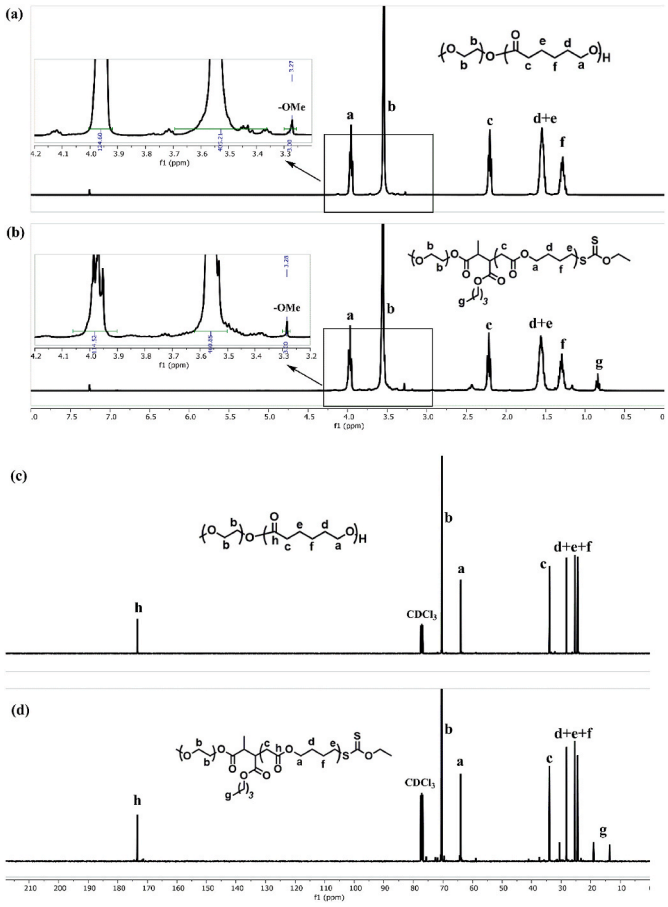

Fig. 1. ^{1}H NMR ($CDCl_3$) spectrum for (a) mPEG-*b*-PCL (b) mPEG-*b*-PMDO. ^{13}C NMR ($CDCl_3$) spectrum for (c) mPEG-*b*-PCL (d) mPEG-*b*-PMDO.

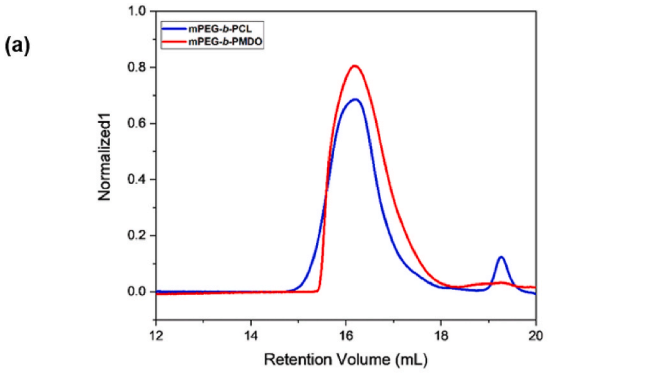

(b)

Polymer	Monomer	M_n[a] (g/mol)	M_n[b] (g/mol)	M_w (g/mol)	$Đ$ (M_w/M_n)
mPEG-*b*-PCL	ε-CL	12,000	8,800	15,300	1.73
mPEG-*b*-PMDO	MDO	11,300	10,100	15,700	1.56

[a]Determined via ^{1}H NMR. [b]Determined from GPC.

Fig. 2. Determining molecular weight distribution and polydispersities ($Đ$) for mPEG-*b*-PCL and mPEG-*b*-PMDO by GPC and ^{1}H NMR analysis (a) GPC graph (b) GPC Characterization table.

b of the methylene protons (-*O*-CH$_2$-CH$_2$-*O*-) of PEG at 3.55 ppm, and peak *a* of the methylene protons (–C(O)–CH$_2$–CH$_2$–CH$_2$–CH$_2$–CH$_2$–*O*-) of CL at 3.96 ppm (refer to magnified spectra in Fig. 1a). Similarly, in Fig. 1b, the ^{1}H NMR spectrum of mPEG-*b*-PMDO (**10**) exhibits an almost similar pattern of peaks for CL and PEG. The DP in PEG and PMDO

blocks was determined in a similar manner to mPEG-*b*-PCL by comparing the peak of the terminal methoxy group (CH$_3$–O–CH$_2$–CH$_2$–*O*-) of PEG, appearing at 3.28 ppm, with peak *b* of the methylene protons (-*O*-CH$_2$-CH$_2$-*O*-) of PEG at 3.55 ppm, and peak *a* of the methylene protons (–CH$_2$–C(O)O–CH$_2$–CH$_2$–CH$_2$–CH$_2$-) of PMDO at 3.98 ppm (refer to magnified spectra in Fig. 1b). Additionally, a peak appeared at the high field region of the spectrum at 0.84 ppm, corresponding to branching groups *g* resulting from backbiting of primary radicals generated at methylene protons during the propagation step of the polymerization (Scheme 1c) [25,43]. The non-stabilized methylene primary radicals generated after the ring-opening of MDO during polymerization steps are susceptible to undergo 1,7-intramolecular hydrogen transfer/1,7-back-biting. This phenomenon has been extensively studied and is commonly observed in the radical polymerization of certain vinyl monomers, such as MDO, to estimate the amount of branching [25,43,44]. The amount of branching in the polymer depends on various polymerization conditions, including reaction temperature and time. For instance, when the reaction is conducted at 65 °C and 70 °C for 24 h, branching levels of 15 % and 13 %, respectively, have been observed [25,44]. Interestingly, limiting the temperature to 50 °C and extending the reaction time to 72 h resulted in an increase in branching to 20 % [43]. In the current study, which was conducted at 70 °C for 48 h, branching was determined to be 16 % based on ^{1}H NMR analysis. Branching in the PMDO block introduces structural irregularities, leading to a higher dispersity in the copolymer [23]. These irregularities disrupt the regular packing of polymer chains, resulting in a more amorphous structure. As a consequence, the copolymer exhibits increased flexibility and a wider range of molecular sizes, contributing to its higher dispersity values. ^{13}C NMR was also supported well from structural analysis in PEG, PCL and PMDO blocks (Fig. 1c and d). The distinguished peak *h* at 173.3 ppm (Fig. 1c) and 173.4 ppm (Fig. 1d) corresponds to carboxylate of CL and MDO respectively, and peak *a* at 63.9 ppm (Fig. 1c) and 64.0 ppm (Fig. 1d) belongs to methylene carbons adjacent to carboxylate of CL and MDO respectively. Refer to pages S8 for the NMR data (^{1}H and ^{13}C) of mPEG-*b*-PCL and mPEG-*b*-PMDO, and pages S9–S10 for the ^{1}H NMR spectra of intermediates **5**, **7**, and **8** in the SI.

To synthesize the required molecular weight of hydrophobic blocks (PCL and PMDO), the appropriate molar ratio of monomers was reacted with the mPEG$_{5k}$ macroinitiator based on their reactivity and conversion. Similar to the determination of DP, molecular weights for PCL and PMDO blocks were calculated using ^{1}H NMR by integrating the corresponding terminal methoxy group peak of mPEG at 3.27 ppm and 3.28 ppm, and the peak of the repeating units of CL/MDO at 3.96 ppm. The molecular weights calculated from ^{1}H NMR (M_n = 12,000 and 11,300 g/mol for mPEG-*b*-PCL and mPEG-*b*-PMDO, respectively) were nearly close to the molecular weights measured from gel permeation chromatography (GPC) analysis (M_n = 8800 and 10,100 g/mol for mPEG-*b*-PCL and mPEG-*b*-PMDO, respectively) (refer to Fig. 2b). However, the observed difference in molecular weights (M_n) determined by ^{1}H NMR and GPC is due to the use of polystyrene standards for calibration in the GPC method. This discrepancy was reflected with the slightly increased corresponding polydispersity values ($Đ$) of 1.73 and 1.56 for mPEG-*b*-PCL and mPEG-*b*-PMDO, respectively. Furthermore, similar variations in M_n between ^{1}H NMR and GPC analyses were consistent across various polymer systems, including homopolymers (e.g., PCL-OH, PCL-Br) and amphiphilic diblock copolymers like poly(ε-caprolactone)-*b*-poly(N-vinylpyrrolidone) (PCL-*b*-PNVP) [45]. The GPC overlay of mPEG-OH and mPEG-*b*-PCL, and mPEG-xanthate and mPEG-*b*-PMDO can be found on page S11 in the SI.

2.2. Solid state properties

We next investigated the solid state properties of mPEG-*b*-PCL (**3**) and mPEG-*b*-PMDO (**10**) by X-ray diffraction (X-RD) and differential scanning calorimetry (DSC) (Fig. 3). Variations in the thermal properties of these block copolymers reveal the differences in the crystallinity of their hydrophobic blocks. X-RD analysis revealed three distinctive diffraction peaks at 2θ = 19°, 21.5°, and 23.5° for both polymers, indicating similar structural features (see Fig. 3a) [46]. The peaks at 2θ = 19° and 23.5°, attributed to the PEG block, displayed clear and prominent signals, suggesting the crystallization of the PEG block in both mPEG-*b*-PCL [46] and mPEG-*b*-PMDO. However, the peak at 2θ = 21.5°, associated with the PCL or PMDO block, exhibited significantly different intensities between the two polymers. In mPEG-*b*-PCL, this peak appeared with robust intensity, indicating crystallization of the PCL block. Conversely, in mPEG-*b*-PMDO, the intensity of this peak was notably weaker, suggesting limited crystallization of the PMDO block. Therefore, this observation implies that the presence of the PMDO block in mPEG-*b*-PMDO contributes to reduced crystallinity or amorphous behaviour of the polymer, whereas the PCL block in mPEG-*b*-PCL exhibits crystalline characteristics. The glass transition temperature (T_g) and melting temperature (T_m) of both polymers are presented in Fig. 3b. T_g values for both mPEG-*b*-PCL and mPEG-*b*-PMDO are comparable, each recorded at −65 °C. However, in contrast to T_g, the T_m of mPEG-*b*-PCL exhibits a higher value of 50 °C with a sharp peak, while T_m of mPEG-*b*-PMDO shows a lower value at 35 °C with a broad peak. The overlay of DSC graphs for mpEG-OH and mPEG-*b*-PCL (refer to page S12 in SI) shows a higher value of T_g and T_m for the PEG block compared to its corresponding mPEG-*b*-PCL, demonstrating the crystalline behaviour of the PEG block. This result is consistent with the X-RD analysis of the PEG block. The lower T_m and broad peak in mPEG-*b*-PMDO indicate disorder in the polymer structure caused by branching, resulting in decreased crystallinity.

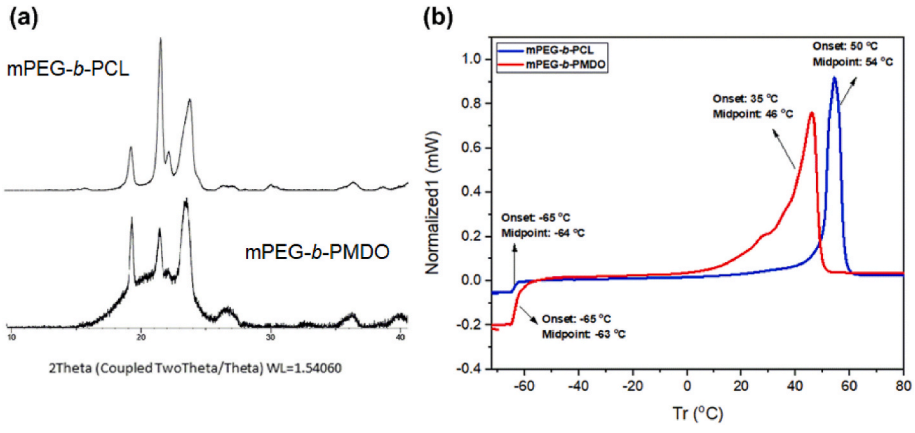

Fig. 3. Solid state properties for mPEG-*b*-PCL and mPEG-*b*-PMDO (a) X-ray diffraction (X-RD) graph (b) Differential scanning calorimetry (DSC) graph.

2.3. NPs synthesis and encapsulation

The amphiphilic diblock copolymers mPEG-*b*-PCL (**3**) and mPEG-*b*-PMDO (**10**) made available in this work were then investigated for self-assembling into spherical NPs that act as potential nanocarriers in drug delivery applications. Initially, well-defined blank particles were achieved by the co-solvent method using dichloromethane (DCM) and ultrapure water (UPH) with a final polymer concentration of 25 mg ml^{-1} in UPH (Table 1). This process enabled the formation of particles composed of a PEG corona (hydrophilic block) and a PCL or PMDO core (hydrophobic block). In this process, initially, a minimum amount of DCM was used for the dissolution of the polymer. Then the polymer solution was added dropwise to UPH while stirring at room temperature, and the stirring continued for 24 h. At this point, polymer dispersion was purified by centrifugation at 3000 rpm for 5 min twice to remove polymer residues that were not self-assembled. The morphology of the resulting pure particles was assessed by dynamic light scattering (DLS) on a Malvern Zetasizer Nanoseries at 25 °C. The DLS data of mPEG-*b*-PCL and mPEG-*b*-PMDO showed the successful formation of spherical blank NPs with an average size of 200 nm, 98 nm with 0.30 and 0.33 polydispersity index (PDI) respectively (refer to S7 and S10, SI). The same procedure was applied for the preparation of curcumin and fenofibrate-loaded NPs from mPEG-*b*-PCL and mPEG-*b*-PMDO (refer to page S7 in the SI for the detailed experimental procedure). The encapsulation was performed with 4 wt% and 10 wt% of curcumin and fenofibrate respectively keeping the final polymer concentration to 25 mg ml^{-1}. The size distribution was recorded for curcumin and fenofibrate-loaded NPs from mPEG-*b*-PCL and mPEG-*b*-PMDO as 168 nm (Figs. S8 and SI), 102 nm (Figs. S11 and SI), 175 nm (Figs. S9 and SI) and 134 nm (Figs. S12 and SI) with 0.33, 0.26, 0.26 and 0.37 PDI respectively.

$$\text{Encapsulation efficiency \% (EE\%)} = \frac{(\textit{Encapsulated amount of actives})(mg)}{(\textit{Initial amount of actives})(mg)}\ X\ 100$$

The NPs with a crystalline core and those with more amorphous core exhibited distinctly different size trends. This variation may stem from differences in hydrophobicity and chain flexibility between PCL and PMDO, which could influence the packing efficiency and morphology of the self-assembled NPs. Moreover, differences in intermolecular interactions and the kinetics of NP formation may also contribute to variations in NP size. For example, in mPEG-*b*-PMDO, the increased hydrophobic interactions within the hydrophobic region led to a reduction in the hydrophobic core compared to its counterpart, mPEG-*b*-PCL (see blank NPs in Table 1). This finding aligns with our recent studies, where NPs formed from poly(vinyl alcohol-*b*-MDO) were also found to be small in size [47]. According to Tables 1 and it can also be observed that after encapsulation, mPEG-*b*-PCL is discovered to have a smaller size as compared to its blank counterpart. The opposite trend is noticed for mPEG-*b*-PMDO whereby after encapsulation, an increase in sizes is detected. The reason for the decrease in size for loaded mPEG-*b*-PCL is speculated to be the actives acting as glue to pack in the hydrophobic core of NPs closely together which resulted in the decrease in size. As for the increase in size for loaded mPEG-*b*-PMDO, our hypothesis is due to the branched structure of mPEG-*b*-PMDO, making it less packable and actives could go into the empty cargo space of the hydrophobic chains, resulting in the increased size. It has been reported that when medium chain triglyceride which inhibits PCL crystallization is introduced into the polymer particle, it profoundly affects drug loading (up to one order increase in loading in certain cases) with very little effect on stability or pharmaco kinetics [48]. In addition, study using as hydrophobic block random copolymers of ε-caprolactone, L-lactide, and ε-decalactone along with PEG as hydrophilic block, yielded particles with higher size, critical micelle concentration (CMC) and stability indicating that such particles with an increase in accessible volume relative to that of a semicrystalline core would be an important rule for tailoring drug delivery properties of such systems [49].

Next, we determined the amount of actives incorporated in NPs core using high-performance liquid chromatography (HPLC). The equations for measuring encapsulation efficiency (EE) and loading efficiency (LE) were described as follows.

$$\text{Drug loading efficiency \% (LE\%)} = \frac{(\textit{Amount of actives})(mg)}{(\textit{total amount of NPs})\ (mg)}\ X\ 100$$

From the EE% analysis, mPEG-*b*-PMDO incorporates nearly 2.2 folds more curcumin than mPEG-*b*-PCL (Table 2). This substantial difference can be attributed to the presence of branching and xanthate end-groups in the PMDO blocks, introduced by RAFT-mediated rROP. These modifications induce higher hydrophobic intermolecular interactions between the PMDO core and curcumin, allowing for greater loading of curcumin into the hydrophobic core of mPEG-*b*-PMDO compared to mPEG-*b*-PCL. Additionally, the regular chain structure of mPEG-*b*-PCL promotes close packing of polymer molecules in the crystalline lamellae, which may hinder the loading of more active compounds, particularly curcumin. On the other hand, mPEG-*b*-PCL can accommodate nearly 1.6 folds more fenofibrate than mPEG-*b*-PMDO. This discrepancy is likely due to the higher flexibility of PCL chains resulting from their linear structure, which facilitates the favourable accommodation of fenofibrate molecules within the PCL core, leading to higher encapsulation. This trend becomes more pronounced with an increase in PCL block size, as its linearity enhances, correlating with an increase in the encapsulated amount of fenofibrate [50]. Interestingly, the LE% analysis

Table 1
Characterization of size for mPEG-*b*-PCL and mPEG-*b*-PMDO NPs before and after encapsulation of curcumin and fenofibrate actives.

Sample name	Z-average (d.nm)					
	Blank	PDI	Curcumin-loaded	PDI	Fenofibrate-loaded	PDI
mPEG-*b*-PCL (**3**)	199.6 ± 4.5	0.3 ± 0.1	167.7 ± 2.0	0.3 ± 0.1	174.6 ± 2.1	0.2 ± 0.1
mPEG-*b*-PMDO (**10**)	98.1 ± 1.4	0.3 ± 0.1	102.3 ± 1.3	0.2 ± 0.1	134.3 ± 1.4	0.3 ± 0.1

Table 2
Encapsulation efficiency (EE) and loading (LE) of mPEG-*b*-PCL and mPEG-*b*-PMDO NPs after encapsulation of curcumin and fenofibrate actives.

Sample name	EE (%)		LE (%)	
	Curcumin-loaded	Fenofibrate-loaded	Curcumin-loaded	Fenofibrate-loaded
mPEG-*b*-PCL (**3**)	48.3	108.2	1.9	10.7
mPEG-*b*-PMDO (**10**)	108.8	65.1	4.3	6.7

revealed higher fenofibrate loading compared to curcumin loading in both mPEG-*b*-PCL and mPEG-*b*-PMDO, with calculated values of 10.7 and 6.7, respectively. This comparative analysis underscores the distinctive encapsulation and loading capacities of mPEG-*b*-PMDO and mPEG-*b*-PCL for curcumin and fenofibrate, providing insight into the influence of structural confirmations between polymer and active compounds. Chemical structures for curcumin and fenofibrate were displayed on page S16 in the SI.

2.4. In vitro release studies

Release studies involve assessing the rate of active compound release from encapsulated particles over a specified duration. The cumulative active release percentages are calculated using the following formula and plotted at given time intervals. *C* and *M* refers to the concentration of actives in the dissolution medium and volume of the dissolution medium respectively.

$$\text{Cumulative amount release} = \frac{(C\,X\,M)\ (mg)}{(\textit{Total amount of actives})(mg)}\ X\ 100$$

In our investigation, *in vitro* release experiments for curcumin and fenofibrate followed a standard protocol utilizing hydro-alcoholic or aqueous sodium dodecyl sulfate (SDS) media [51,52]. These media provide a physiologically relevant environment that enhances the solubility and controlled release of active molecules, thereby improving its therapeutic potential. Both curcumin and fenofibrate are hydrophobic molecules with poor solubility in water alone, which can restrict their bioavailability and efficacy. Therefore, the addition of ethanol or SDS aids in solubilizing these actives and facilitating their release from the NPs. The results of our study on the *in vitro* release of free curcumin or curcumin from NPs of mPEG-*b*-PCL and mPEG-*b*-PMDO after incubation in UPH: Ethanol = 1:1 dissolution medium (200 mL), and free fenofibrate or fenofibrate from NPs of mPEG-*b*-PCL and mPEG-*b*-PMDO after incubation in 0.5 wt% SDS solution (200 mL) using dialysis bag (Spectra/Por, 12000–14000 Da MWCO) each at 37 °C for 24 h under 100 rpm stirring, are presented in Figs. 4 and 5, respectively. After encapsulation, each sample was divided into triplicates, and these sets of triplicates were subjected to the corresponding dissolution medium to ensure consistency. To maintain sink conditions, fresh dissolution medium was replaced after each sampling (refer to page S7 in the SI for the detailed experimental procedure). Samplings were taken at pre-determined time intervals and quantified using HPLC. During the release experiment, a gradual increase in the release of curcumin up to 56 % and 27 %, and fenofibrate up to 54 % and 18 % was observed from NPs of mPEG-*b*-PCL and mPEG-*b*-PMDO respectively in 5 h period. After 24 h, over 100 % and 61 % of encapsulated curcumin, and 66 % and 30 % of encapsulated fenofibrate were released from NPs of mPEG-*b*-PCL and mPEG-*b*-PMDO respectively. It was also found that the release of both actives from mPEG-*b*-PMDO was slower than the release from mPEG-*b*-PCL, which may be attributed to the amorphous character in mPEG-*b*-PMDO

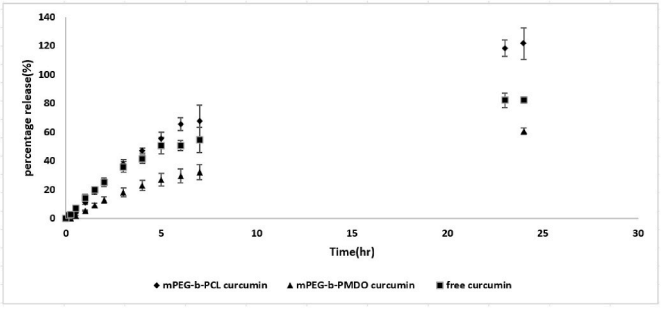

Fig. 4. The cumulative release profile for free curcumin and curcumin encapsulated mPEG-*b*-PCL and mPEG-*b*-PMDO NPs (each graph is from the average of three repetitions).

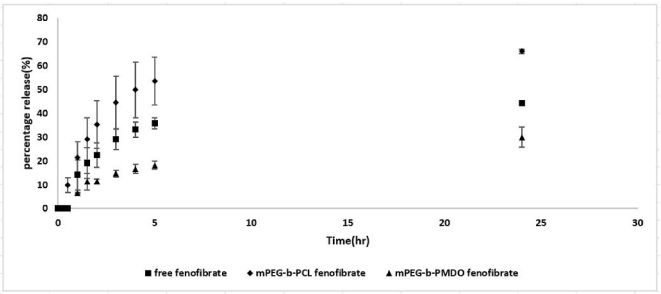

Fig. 5. The cumulative release profile for free fenofibrate and fenofibrate encapsulated mPEG-*b*-PCL and mPEG-*b*-PMDO NPs (each graph is from the average of three repetitions).

resulting in more hydrophobic interactions between the polymer and actives, thus accounting for the slower release of curcumin and fenofibrate. In contrast, release of free curcumin and fenofibrate was observed as 51 % and 36 %, respectively, after 5 h. Approximately 80 % of curcumin and 45 % of fenofibrate were released after 24 h (refer to page S16 in SI for individual free release graphs). Interestingly, it was observed that the release of curcumin and fenofibrate from mPEG-*b*-PCL NPs occurred even faster than that of the free actives. This phenomenon may be attributed to the uniform distribution of actives in the crystalline core of mPEG-*b*-PCL NPs, promoting faster release. Conversely, in the case of mPEG-*b*-PMDO, the actives were released slowly and consistently due to increased hydrophobic interactions within the amorphous core of mPEG-*b*-PMDO NPs. Our study reveals that the optimum and controlled release of curcumin and fenofibrate from mPEG-*b*-PMDO amphiphilic diblock copolymer could serve as a model system to establish conditions for a variety of actives in personal care applications.

3. Conclusion

In this study, the amphiphilic diblock copolymers, namely mPEG-*b*-PCL and mPEG-*b*-PMDO, with comparable molecular weights of hydrophilic and hydrophobic blocks, were synthesized through acid-catalyzed ROP of CL (ε-caprolactone) and reversible addition–fragmentation chain transfer (RAFT)-mediated rROP of MDO (2-methylene-1,3-dioxepane), respectively. The degree of polymerization and molecular weight distribution (M_n) of both block copolymers were determined using ^{1}H NMR and GPC techniques, however, the observed difference in M_n is due to the use of polystyrene standards for calibration in the GPC method. During the rROP of MDO, a side reaction involving 1,7-intramolecular hydrogen transfer/1,7-back-biting led to branching in the polymer chain. The extent of branching was found to depend on various polymerization conditions such as reaction temperature and time, with approximately 16 % branching observed based on ^{1}H NMR analysis. These copolymers were then employed to encapsulate hydrophobic actives, curcumin, and fenofibrate, with the aim of enhancing water solubility, stability, and controlling release profiles. The PCL segment in mPEG-*b*-PCL and the PMDO segment in mPEG-*b*-PMDO exhibited crystalline and more amorphous characteristics, respectively. Notably, the amorphous mPEG-*b*-PMDO demonstrated superior encapsulation efficiency for curcumin compared to its crystalline counterpart, mPEG-*b*-PCL, while mPEG-*b*-PCL exhibited higher encapsulation efficiency for fenofibrate. Both copolymers showed higher loading efficiency for fenofibrate than curcumin, attributed to structural differences influencing interactions between the polymer and active compounds, such as the branching structure in PMDO and the higher flexibility of the linear structure in PCL. In both cases of curcumin and fenofibrate, utilizing rROP-derived PEG-*b*-PMDO resulted in slow and controlled *in vitro* release of the active compounds. This underscores two key advantages: Firstly, the more amorphous nature of PEG-*b*-PMDO, attributed to the PMDO block, offers control over amorphous characteristics by

modulating branching density through varying reaction conditions including monomer proportions and radical flux. Secondly, synthesizing PEG-*b*-PMDO via rROP proves more straightforward in an industrial setting compared to condensation polymerization. Additionally, radical-based polymerizations are more amenable to incorporating functionalities such as targeting moieties, compared to condensation polymerization. In conclusion, mPEG-*b*-PMDO and, by extension, rROP-derived block copolymers emerge as effective "(bio)degradable alternatives" for formulating hydrophobic actives with precise release manipulation requirements. The ease of implementation and versatility of radical-based polymerization make mPEG-*b*-PMDO a promising candidate for controlled release technology in pharmaceutical and care chemical fields. Ongoing research aims to explore various rROP-derived block copolymer structures in nanoparticle formulations with other sensitive actives to broaden applications in controlled release technology.

CRediT authorship contribution statement

Algin Oh Biying: Validation, Methodology, Formal analysis. **Srinivasa Reddy Mothe:** Writing – original draft, Methodology, Formal analysis, Data curation, Conceptualization. **Alexander W. Jackson:** Validation, Methodology, Formal analysis, Conceptualization. **Parijat Kanaujia:** Validation, Supervision, Formal analysis, Data curation, Conceptualization. **Praveen Thoniyot:** Writing – review & editing, Supervision, Resources, Project administration, Investigation, Funding acquisition, Data curation, Conceptualization.

Declaration of competing interest

The authors declare that they have no conflict of interest.

Data availability

Data will be made available on request.

Acknowledgments

We gratefully acknowledge the Agency for Science, Technology and Research (A*STAR), Singapore; Science and Engineering Research Council (SERC), Singapore, under Specialty Chemicals AME IAF-PP Programme Grant A1786a0025. We thank Lohitha Rao Chennamaneni for monomer supply and Wenguang Zhao for assistance with GPC analysis.

Appendix A. Supplementary data

Supplementary data to this article can be found online at https://doi.org/10.1016/j.polymer.2024.127284.

References

[1] D.D. Lasic, Doxorubicin in sterically stabilized liposomes, Nature 380 (1996) 561–562.
[2] M. Yokoyama, Novel Passive Targetable Drug Delivery with Polymeric Micelles. Biorelated Polymers and Gels: Controlled Release and Applications in Biomedical Engineering, 1998.
[3] R. Duncan, Drug-polymer conjugates: potential for improved chemotherapy, Anti Cancer Drugs 3 (1992) 175–210.
[4] P. Couvreur, F. Puisieux, Nano-and microparticles for the delivery of polypeptides and proteins, Adv. Drug Deliv. Rev. 10 (1993) 141–162.
[5] K. Akiyoshi, S. Kobayashi, S. Shichibe, D. Mix, M. Baudys, S.W. Kim, J. Sunamoto, Self-assembled hydrogel nanoparticle of cholesterol-bearing pullulan as a carrier of protein drugs: complexation and stabilization of insulin, J. Contr. Release 54 (1998) 313–320.
[6] E. Allemann, R. Gurny, E. Doelker, Drug-loaded nanoparticles: preparation methods and drug targeting issues, Eur. J. Pharm. Biopharm. 39 (1993) 173–191.
[7] J. Zou, Y. Yu, Y. Li, W. Ji, C. Chen, W. Law, P.N. Prasad, C. Cheng, Well-defined diblock brush polymer–drug conjugates for sustained delivery of paclitaxel, Biomater. Sci. 3 (2015) 1078–1084.
[8] H. Cabral, K. Kataoka, Progress of drug-loaded polymeric micelles into clinical studies, J. Contr. Release 190 (2014) 465–476.
[9] H. Yoon, W. Jang, Polymeric supramolecular systems for drug delivery, J. Mater. Chem. 2 (2010) 211–222.
[10] W. Scarano, P.D. Souza, M.H. Stenzel, Dual-drug delivery of curcumin and platinum drugs in polymeric micelles enhances the synergistic effects: a double act for the treatment of multidrug-resistant cancer, Biomater. Sci. 3 (2015) 163–174.
[11] K. Miller, C. Clementi, D. Polyak, A. Eldar-Boock, L. Benayoun, I. Barshack, Y. Shaked, G. Pasut, R. Satchi-Fainaro, Poly (ethylene glycol)–paclitaxel–alendronate self-assembled micelles for the targeted treatment of breast cancer bone metastases, Biomaterials 34 (2013) 3795–3806.
[12] S. Cajot, P. Lecomte, C. Jérôme, R. Riva, Novel functional degradable block copolymers for the building of reactive micelles, Polym. Chem. 4 (2013) 1025–1037.
[13] A.A. Samad, Y. Bakkour, C. Fanny, F.E. Omar, J. Coudane, B. Nottelet, From nanospheres to micelles: simple control pf PCL-g-PEG copolymers' amphiphilicity through thiol-yne photografting, Polym. Chem. 6 (2015) 5093–5102.
[14] M. Jones, J. Leroux, Polymeric micelles - a new generation of colloidal drug carriers, Eur. J. Pharm. Biopharm. 48 (1999) 101–111.
[15] L. Glavas, P. Olsén, K. Odelius, A. Albertsson, Achieving micelle control through core crystallinity, Biomacromolecules 14 (2013) 4150–4156.
[16] P. Grossen, D. Witzigmann, S. Sieber, J. Huwyler, PEG-PCL-based nanomedicines: a biodegradable drug delivery system and its application, J. Contr. Release 260 (2017) 46–60.
[17] H. Danafar, S. Davaran, K. Rostamizadeh, H. Valizadeh, M. Hamidi, Biodegradable m-PEG/PCL core-shell micelles: preparation and characterization as a sustained release formulation for curcumin, Adv. Pharmaceut. Bull. 4 (2014) 501.
[18] A.W. Jackson, Reversible-deactivation radical polymerization of cyclic ketene acetals, Polym. Chem. 11 (2020) 3525–3545.
[19] P. Xu, X. Huang, X. Pan, N. Li, J. Zhu, X. Zhu, Hyperbranched polycaprolactone through RAFT polymerization of 2-methylene-1, 3-dioxepane, Polymers 11 (2019) 318.
[20] G. Hedir, Functional Degradable Polymers via RAFT/MADIX Mediated Polymerization of Cyclic Ketene Acetals and Vinyl Monomers, University of Warwick, 2016. PhD diss.
[21] C.A. Bell, G.G. Hedir, R.K. O'Reilly, A.P. Dove, Controlling the synthesis of degradable vinyl polymers by xanthate-mediated polymerization, Polym. Chem. 6 (2015) 7447–7454.
[22] G.G. Hedir, C.A. Bell, N.S. Ieong, E. Chapman, I.R. Collins, R.K. O'Reilly, A.P. Dove, Functional degradable polymers by xanthate-mediated polymerization, Macromolecules 47 (2014) 2847–2852.
[23] G. Hedir, C. Stubbs, P. Aston, A.P. Dove, M.I. Gibson, Synthesis of degradable poly (vinyl alcohol) by radical ring-opening copolymerization and ice recrystallization inhibition activity, ACS Macro Lett. 6 (2017) (2017) 1404–1408.
[24] W.J. Bailey, Z. Ni, S.R. Wu, Synthesis of poly-ϵ-caprolactone via a free radical mechanism. Free radical ring-opening polymerization of 2-methylene-1, 3-dioxepane, J. Polym. Sci. Polym. Chem. Ed. 20 (1982) 3021–3030.
[25] S.R. Mothe, J.S.J. Tan, L.R. Chennamaneni, F. Aidil, Y. Su, H.C. Kang, F.C.H. Lim, P. Thoniyot, A systematic investigation of the ring size effects on the free radical ring-opening polymerization (rROP) of cyclic ketene acetal (CKA) using both experimental and theoretical approach, J. Polym. Sci. 58 (2020) 1728–1738.
[26] X. Shuai, H. Ai, N. Nasongkla, S. Kim, J. Gao, Micellar carriers based on block copolymers of poly (ε-caprolactone) and poly (ethylene glycol) for doxorubicin delivery, J. Contr. Release 98 (2004) 415–426.
[27] Y. Niyom, A.E. Flood, D. Crespy, Review of crystallization in nanoconfinement created by emulsions and microemulsions for pharmaceutical applications, ACS Appl. Nano Mater. 6 (2023) 21451–21461.
[28] Z. Ma, A. Haddadi, O. Molavi, A. Lavasanifar, Micelles of poly(ethylene oxide)-b-poly(e-caprolactone) as vehicles for the solubilization, stabilization, and controlled delivery of curcumin, J. Biomed. Mater. Res. 86A (2007) 300–310.
[29] S. Rathore, M. Mukim, P. Sharma, S. Devi, J.C. Nagar, M. Khalid, Curcumin: a review for health benefits, Int. J. Res. Rev. 7 (2020) 273–290.
[30] J. Gómez-Estaca, M.P. Balaguer, G. López-Carballo, R. Gavara, P. Hernández-Muñoz, Improving antioxidant and antimicrobial properties of curcumin by means of encapsulation in gelatin through electrohydrodynamic atomization, Food Hydrocolloids 70 (2017) 313–320.
[31] F.A. Rheim, A.A. Ragab, F.M. Hammam, H.E. Hamdy, Evaluation of DNA damage in vivo by comet assay and chromosomal aberrations for pyrethroid insecticide and the antimutagenic role of curcumin. Egypt, J. Hosp. Med. 59 (2015) 172–181.
[32] A. Noorafshan, S. Ashkani-Esfahani, A review of therapeutic effects of curcumin, Curr. Pharmaceut. Des. 19 (2013) 2032–2046.
[33] S. Prasad, A.K. Tyagi, B.B. Aggarwal, Recent developments in delivery, bioavailability, absorption and metabolism of curcumin: the golden pigment from golden spice, Cancer Res Treat 46 (2014) 2–18.
[34] S.C. Gupta, S. Patchva, B.B. Aggarwal, Therapeutic roles of curcumin: lessons learned from clinical trials, AAPS J. 15 (2013) 195–218.
[35] S.J. Hewlings, D.S. Kalman, Curcumin: a review of its effects on human health, Foods 6 (2017) 92–102.
[36] G.M. Keating, K.F. Croom, Fenofibrate: a review of its use in primary dyslipidaemia, the metabolic syndrome and type 2 diabetes mellitus, J. Mol. Med. 67 (2007) 121–153.
[37] R. Kumar, Solubility and bioavailability of fenofibrate nanoformulations, ChemistrySelect 5 (2020) 1478–1490.
[38] R.L. Ellen, R. McPherson, Long-term efficacy and safety of fenofibrate and a statin in the treatment of combined hyperlipidemia, Am. J. Cardiol. 81 (1998) 60B–65B.

[39] J. Shepherd, The fibrates in clinical practice: focus on micronized fenofibrate, Atherosclerosis 110 (1994) S55–S63.
[40] C.W. Shong, C.H. Sow, A.T. S Wee, Science at the Nanoscale: an Introductory Textbook, Pan Stanford Publishing, 2010.
[41] J. Heller, R. Sparer, G. Zentner, M. Chasin, R. Langer, Biodegradable Polymers as Drug Delivery Systems, Marcel Dekker, New York, 1990.
[42] G.S. Kwon, M. Naito, K. Kataoka, M. Yokoyama, Y. Sakurai, T. Okano, Block copolymer micelles as vehicles for hydrophobic drugs, Colloids Surf. B Biointerfaces 2 (1994) 429–434.
[43] S. Jin, K.E. Gonsalves, A study of the mechanism of the free-radical ring-opening polymerization of 2-methylene-1, 3-dioxepane, Macromolecules 30 (1997) 3104.
[44] J.B. Lena, A.W. Jackson, L.R. Chennamaneni, C.T. Wong, F. Lim, Y. Andriani, P. Thoniyot, A.M.V. Herk, Degradable poly (alkyl acrylates) with uniform insertion of ester bonds, comparing batch and semibatch copolymerizations, Macromolecules 53 (2020) 3994–4011.
[45] A.K. Mishra, V.K. Patel, N.K. Vishwakarma, C.S. Biswas, M. Raula, A. Misra, T. K. Mandal, B. Ray, Synthesis of well-defined amphiphilic poly (ε-caprolactone)-b-poly (N-vinylpyrrolidone) block copolymers via the combination of ROP and xanthate-mediated raft polymerization, Macromolecules 44 (2011) 2465–2473.
[46] J. Sun, C. He, X. Zhuang, X. Jing, X. Chen, The crystallization behavior of poly (ethylene glycol)-poly (ε-caprolactone) diblock copolymers with asymmetric block compositions, J. Polym. Res. 18 (2011) 2161–2168.
[47] S.R. Mothe, P. Kanaujia, A.B.Y. Oh, P. Ang, P. Thoniyot, PVA free-radical diblock copolymer for nanoencapsulation with enhanced biodegradability in the environment, Eur. Polym. J. 196 (2023) 112287.
[48] J. Gou, S. Feng, H. Xu, G. Fang, Y. Chao, Y. Zhang, H. Xu, X. Tang, Decreased core crystallinity facilitated drug loading in polymeric micelles without affecting their biological performances, Biomacromolecules 16 (2015) 2920–2929.
[49] L. Glavas, P. Olsén, K. Odelius, A.C. Albertsson, Achieving micelle control through core crystallinity, Biomacromolecules 14 (2013) 4150–4156.
[50] K.K. Jette, D. Law, E.A. Schmitt, G.S. Kwon, Preparation and drug loading of poly (ethylene glycol)-block-poly (ε-caprolactone) micelles through the evaporation of a cosolvent azeotrope, Pharmaceut. Res. 21 (2004) 1184–1191.
[51] M.M.A. Nasra, H.M. Khiri, H.A. Hazzah, O.Y. Abdallah, Formulation, in-vitro characterization and clinical evaluation of curcumin in-situ gel for treatment of periodontitis, Drug Deliv. 24 (2017) 133–142.
[52] S. Wei, J. Ren, N. Li, W. Huo, C. Gao, Preparation and pharmacokinetic study of fenofibrate cubic liquid crystalline, Asian J. Pharm. Sci. 12 (2017) 580–585.